# Evidence for large-scale structures in granular superconductors

S. A. Dodds and S. N. Harrington*
*Physics Department, Rice University, Houston, Texas 77251*

R. S. Newrock and K. Loeffler†
*Physics Department, University of Cincinnati, Cincinnati, Ohio 45221*
(Received 20 August 1984; revised manuscript received 8 August 1985)

We have made measurements of the temperature and angular dependence of the critical field for superconductivity in thin-film specimens of Al:$Al_2O_3$ composites. The measurements lead us to infer that these specimens are composed of one or more layers with thicknesses between the grain size and the overall film thickness. This inference is corroborated by measurements of the fluctuation conductivity. Preliminary data on Al:Te composite films suggest that nonrandom structures of similar scale are also present in this material.

## I. INTRODUCTION

Materials which are strongly disordered (amorphous or granular) and specimens in which one or more spatial dimensions are small (thin films or whiskers) have been of interest for many years. Initially, superconducting systems were used to explore thermal fluctuations near the critical temperature. These become observable if the material is sufficiently disordered or a dimension is sufficiently small.[1] More recently, a number of workers have used disordered materials to study several topics of current interest, particularly the Kosterlitz-Thouless transition,[2] localization phenomena,[3] and metal-insulator transitions.[4] The present paper is concerned, in particular, with the characterization of granular aluminum, a disordered material used in some of these investigations. More generally, the methods presented here could be applied to many superconducting composite materials.

Granular aluminum is formed by evaporating or sputtering aluminum in an oxygen-containing atmosphere or by co-depositing it with an immiscible nonmetal. With this technology it is relatively easy to make film specimens with a wide range of resistivities and thicknesses. Dark-field electron microscopy shows that the specimens are composed of small (20—100 Å diameter) aluminum grains dispersed in a matrix of aluminum oxide or co-deposited material.[5] This microstructure is similar to that of granular materials formed with other metals.[6]

Because granular aluminum is a random composite, it is important to consider the possibility that, within any particular specimen, there may be systematic variations in grain size, grain properties, intergrain coupling, or all of these. The possible effects of such variations on the properties of the superconducting state have been recognized by several authors.[7,8] In most cases the concern has been with small variations about the average, occurring on length scales small compared to the specimen size. Other measurements[9,10] suggest that there may be more drastic variations extending across a significant fraction of the specimen. In particular, measurements of the angular dependence of the superconducting critical field in some Al:$Al_2O_3$ films have been interpreted in terms of a layer structure.[9]

Here we report extensive new measurements in the Al:$Al_2O_3$ system, and preliminary results in the Al:Te system, with particular emphasis on the anisotropy and temperature dependence of the critical field for superconductivity. Although it is not possible to account for all the details of these measurements with the simplified models used, the present work extends and confirms the main conclusion of Ref. 9: some form of large-scale structure may be present in composite films. Measurements of the fluctuation conductivity above the critical temperature corroborate this inference. Furthermore, the presence of large-scale variations has been demonstrated in a number of films from three different evaporators and for two different compositions. At least two earlier studies[10] independently found similar anisotropies in the critical fields of Al:$Al_2O_3$ films. It is likely, therefore, that the types of structure we observe are intrinsic to these systems and not an accident of our preparation methods.

To understand other properties of these composite materials it is very helpful to know of the existence of variations in the parameters of the material on all length scales. In many systems, relatively large-scale variations can be detected by measuring the anisotropy and temperature dependence of the superconducting critical field.

In the next section we summarize the models we will use to analyze our critical-field and fluctuation-conductivity data. In Sec. III we describe the sample-preparation and measurement techniques. Our results for the Al:$Al_2O_3$ system are in Sec. IV, while a brief presentation of the preliminary Al:Te data is in Sec. V. The last section contains our conclusions.

## II. SUMMARY OF MODELS

Macroscopic anisotropy of the critical field for superconductivity can be caused by the geometry of the sample or by effects intrinsic to the material. As examples of geometric effects we will consider films thin compared to the coherence length, small cylinders which might arise

 

during film growth under conditions of limited atomic mobility, and the possibility of surface superconductivity in thick samples. Intrinsic effects could arise from certain types of Fermi-surface anisotropy,[11] or from the presence of numerous coherently coupled layers within the specimen. We consider each of these possibilities in turn, summarizing the results in Table I. Geometric and intrinsic effects are not, of course, mutually exclusive and might be present in the same specimen.

For an isotropic type-II film, thin compared to the coherence length $\xi(T)$, a Ginzburg-Landau treatment leads to an implicit expression[12] for the angular dependence of the critical field:

$$H_c(\theta)\frac{\sin\theta}{H_{cz}}+\left[H_c(\theta)\frac{\cos\theta}{H_{ct}}\right]^2=1\ . \tag{1}$$

The angle $\theta$ is measured with respect to the plane of the film. This expression predicts a cusp in the angular dependence when the field is nearly parallel to the plane of the film ($\theta=0$). The critical fields for parallel and perpendicular orientations are related to $\xi(T)$ and the film thickness $d$ by

$$H_c(\theta=0)=H_{ct}=\sqrt{12}\frac{\phi_0}{2\pi d\xi(T)} \tag{2}$$

and

$$H_c(\theta=\pi/2)=H_{cz}=\frac{\phi_0}{2\pi\xi^2(T)}\ , \tag{3}$$

where $\phi_0$ is the flux quantum. (We specify the critical fields for the directions transverse and parallel to the $z$ axis, arbitrarily taken to be the normal to the film in these isotropic materials. In other cases the $z$ axis will be taken along a symmetry direction. This notation allows us to reserve the symbols $H_{c\parallel}$ and $H_{c\perp}$ for critical fields parallel and perpendicular to the surface of the actual film specimen. The distinction is important when the relation between symmetry axes or material anisotropy axes and the film surface is unknown.) Since $\xi(T)=\xi(0)(1-T/T_c)^{-1/2}$ below $T_c$, these equations predict a linear temperature dependence for $H_{cz}$ and a parabolic dependence for $H_{ct}$. The ratio $H_{cz}/H_{ct}=d/\sqrt{12}\xi(T)$ will also be temperature dependent. These results are shown in the first row of Table I.

Equations (2) and (3) can be used to estimate various parameters from the measured critical field data. The temperature-dependent coherence length $\xi(T)$ can be estimated directly from Eq. (3), while the zero-temperature coherence length $\xi(0)$ can be found from Eq. (3) or from the slope $dH_{cz}/dT$, if $T_c$ is known. Similarly, the film thickness can be found from Eq. (2), or from the ratio $H_{cz}/H_{ct}$, once $\xi(T)$ is known. Equations (2) and (3) also predict the relation

$$\frac{H_{cz}}{H_{ct}}=\left[\frac{\pi d^2}{6\phi_0}\right]^{1/2}H_{cz}^{1/2}\ , \tag{4}$$

from which $d$ can be found directly if the ratio $H_{cz}/H_{ct}$ is plotted against $H_{cz}^{1/2}$.

A different geometry will be of interest in our consideration of the Al:Te data. In the Appendix we derive the critical fields for a right circular cylinder of radius $R$, assumed small compared to $\xi(T)$. If angles are measured from a plane perpendicular to the cylinder axis, we can write the result as

$$\left[H_c(\theta)\frac{\sin\theta}{H_{cz}}\right]^2+\left[H_c(\theta)\frac{\cos\theta}{H_{ct}}\right]^2=1\ . \tag{5}$$

The transverse and $z$-axis critical fields are, respectively,

$$H_c(\theta=0)=H_{ct}=\frac{\phi_0}{\pi R\xi(T)} \tag{6}$$

and

$$H_c(\theta=\pi/2)=H_{cz}=\sqrt{2}H_{ct}\ . \tag{7}$$

This differs from the thin-film result in several important aspects. First, the angular variation is smooth around the maximum critical field, rather than cusped. Second, both $H_{cz}$ and $H_{ct}$ exhibit a parabolic temperature dependence, and their ratio is constant. Finally, critical-field data alone cannot be used to obtain estimates of $R$ or $\xi(T)$. These results comprise the second row of Table I.

Thick specimens of isotropic material will exhibit an anisotropic critical field, due to surface superconductivity, if they have a planar surface. When the applied field is perpendicular to the surface, the critical field is $H_{cz}=H_{c2}$ of the bulk material, given by Eq. (3). When the field is parallel to the surface, the critical field measured by resistivity is that of the surface sheath, given by $H_{ct}=H_{c3}=1.69H_{c2}$. The angular dependence near the parallel orientation is difficult to evaluate, but the slope is known to be finite at $\theta=0$, implying a cusp qualitatively similar to the thin-film case.[13] The temperature dependence of both $H_{ct}$ and $H_{cz}$ is predicted to be linear and therefore $H_{cz}/H_{ct}=0.59$, independent of temperature. These results are shown in the third row of Table I.

In the intermediate-thickness regime the two surface sheaths interact and $H_{ct}$ is a complicated function of $d/\xi(T)$. Numerical calculations[14] of $H_{ct}$, shown in Fig. 1, indicate that the thin-film results are accurate for

TABLE I. Critical-field models near $T_c$, neglecting paramagnetic effects. (2D and 3D denote two and three dimensional.)

| Model | $H_c(\theta)$ | $H_{cz}(T)$ | $H_{ct}(T)$ | $H_{cz}(T)/H_{ct}(T)$ |
|---|---|---|---|---|
| 2D isotropic | cusp | linear | parabolic | $\propto d/\xi(T)$ |
| Cylinders | bump | parabolic | parabolic | $\sqrt{2}$ |
| 3D isotropic | $H_{c3}$ | linear | linear | 0.59 |
| 3D anisotropic | $H_{c3}$ | linear | linear | $0.59H_c(\theta')$ |

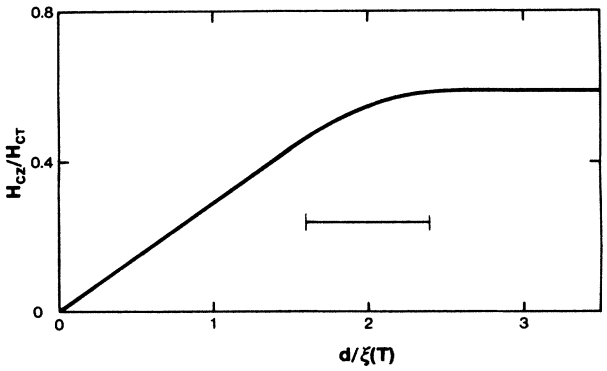


FIG. 1. Plot of $H_{cz}/H_{ct}$ vs $d/\xi(T)$ for an isotropic thin film. The bar marks the two- to three-dimensional transition (Ref. 14). The plateau is due to surface superconductivity when the specimen is sufficiently thick.

$\xi(T)/d \geq 0.6$, while the thick-sample results hold for $\xi(T)/d \leq 0.4$. We also note that $d/\xi(T) \propto H_{cz}^{1/2}$, so that the plot of $H_{cz}/H_{ct}$ versus $H_{cz}^{1/2}$ suggested by Eq. (4) should also look like Fig. 1, with the two- to three-dimensional transition occurring over a well-defined range of $H_{cz}^{1/2}$ values. We will use this fact to check the consistency of our estimates of $\xi(T)$ and $d$ for those films where measurements extend to large enough fields.

We model an intrinsically anisotropic superconductor by introducing an anisotropy in the Ginzburg-Landau coherence length. In the literature such models have been used to describe layered materials with strong interlayer coupling, but we do not imply any mechanism at this point in the discussion. Assume that the material has a preferred axis, along which the coherence length is $\xi_z(T)$. The coherence length transverse to the preferred axis is denoted by $\xi_t(T)$. If angles are measured from the transverse plane, the critical fields are given by Eq. (5), when the transverse and $z$-axis critical fields are given by[15,16]

$$H_c(\theta=0)=H_{ct}=\frac{\phi_0}{2\pi\xi_t(T)\xi_z(T)} , \tag{8}$$

$$H_c(\theta=\pi/2)=H_{cz}=\frac{\phi_0}{2\pi\xi_t^2(T)} . \tag{9}$$

The angular dependence of the critical field is evidently identical to that for cylinders of isotropic material, but the temperature dependence is linear in this case, rather than parabolic. The critical field ratio $H_{cz}/H_{ct}=\xi_z(T)/\xi_t(T)$ is a constant of the material, independent of temperature.

A thick specimen of anisotropic material will exhibit surface superconductivity when the applied field is parallel to a flat surface of the sample. As in isotropic materials $H_{c3}=1.69H_{c2}$, but $H_{c2}$ is given[16] by Eq. (5). Depending on the orientation of the surface relative to the material axes, the measured critical-field ratio may be larger or smaller than the ratio intrinsic to the material. These results complete Table I.

Many of our specimens have rather large critical fields, so one should consider the limit imposed by the spin paramagnetism of the electrons. The primary consequence of electron spin is to lower the values of $H_{c2}(T)$ and decrease the ratio $H_{c3}/H_{c2}$, relative to the no-spin situation. Both of these effects have been described in detail by St. James.[13] In a plot like Fig. 1, the most readily observable result would be to raise the level of the plateau at large $d/\xi(T)$. The magnitude of the paramagnetic effects is determined by a quantity $\alpha$, given by

$$\alpha=\sqrt{2}\frac{H_{c2}(0)}{H_p(0)} , \tag{10}$$

where $H_{c2}(0)$ is the bulk critical field in the absence of spin paramagnetism and $H_p(0)$ is the paramagnetic limiting field, both at $T=0$. These quantities are related to the gap energy $\Delta_0$ by

$$H_{c2}(0)=\frac{\Delta_0\phi_0}{16k_BT_c\xi^2(0)}\approx 0.109\frac{\phi_0}{\xi^2(0)} \tag{11}$$

and

$$H_p(0)=\frac{\Delta_0}{\sqrt{2}\mu_B}\approx 18.6\left[\frac{\text{kOe}}{\text{K}}\right]T_c , \tag{12}$$

where we have used the BCS relation $\Delta_0 \approx 1.76k_BT_c$. Equations (10)–(12) will be used to estimate $\alpha$ from experimentally determined quantities.

An additional complication is introduced by the presence of spin-orbit scattering in the sample. The spin-orbit scattering reduces the difference in spin susceptibility between the normal and superconducting states, thereby raising the critical fields toward their zero-spin values.[11] The spin-orbit scattering time has been estimated from tunneling measurements in clean aluminum films, but the effect does not seem to be large enough to explain the critical-field data on the same films.[17] It is also reasonable to assume that the scattering time depends on details of sample preparation. Because of these uncertainties, we will not attempt a quantitative analysis of our results in the field and temperature region where paramagnetic limiting is likely to be significant.

As noted in the Introduction, the fluctuation-induced conductivity was an early motivation for the study of disordered systems. The fluctuation conductivity, $\sigma_{fl}=\sigma-\sigma_n$, is defined as the excess above the normal-state conductivity $\sigma_n$ due to superconducting fluctuations above $T_c$. Testardi *et al.*[7] have expressed the standard Aslamazov-Larkin (AL) result[18] in a particularly convenient form for dirty isotropic superconductors

$$\sigma_{AL}=\frac{e^2}{32\hbar d\tau}\left[1+\frac{d}{\xi(T)}\coth\left[\frac{d}{\xi(T)}\right]\right] , \tag{13}$$

where $\tau=(T_c-T)/T_c$. This expression is valid when $\sigma_{fl}/\sigma_n \ll 1$. For very thick or very thin samples, Eq. (13) reduces to the usual "three-dimensional" or "two-dimensional" forms.

The AL treatment is adequate in sufficiently dirty materials, but other contributions to $\sigma_{fl}$ are significant in cleaner specimens. These additions are usually referred to as Maki-Thompson (MT) terms. For a specimen of thickness $d$, the additional conductivity is given by[19]

$$\sigma_{\mathrm{MT}}=\frac{e^2}{8\hbar d(\tau-\delta)}\left\{\ln\left[\frac{\xi(0)}{d\delta^{1/2}}\sinh\left[\frac{d\tau^{1/2}}{\xi(0)}\right]\right]+\tfrac{1}{2}\ln\left[\frac{\tau}{\delta}\right]\right\}. \quad (14)$$

The parameter $\delta$ specifies the strength of a pair breaker, which is needed to suppress divergences in the calculation for one- and two-dimensional specimens. Empirically, $\delta$ increases with the resistivity of the film.[1] In this approximation, the total fluctuation conductivity is given by

$$\sigma_{\mathrm{fl}}=\sigma_{\mathrm{AL}}+\sigma_{\mathrm{MT}}\,. \quad (15)$$

The region of validity for Eq. (14) is somewhat smaller than that for Eq. (13). When $\xi(T)\gg d$, we require $\sigma_{\mathrm{fl}}/\sigma_n\ll\delta$, while in the limit $\xi(T)\ll d$ the condition $\sigma_{\mathrm{fl}}/\sigma_n\ll(\tau\delta)^{1/2}$ is required.

The arbitrary introduction of $\delta$ in the MT calculation is somewhat unsatisfactory. Detailed microscopic calculations by Patton[20] and by Keller and Korenman[21] have shown how the divergences can be removed by a careful treatment of impurity scattering. For two-dimensional films $\sigma_{\mathrm{fl}}$ can be expressed[20] in the MT form with a weakly-temperature-dependent $\delta$. The expected temperature dependence has been directly demonstrated in Al films,[22] and other features of the Patton model have been confirmed in several thin-film systems.[23] Numerical comparisons of Eq. (15) with the Patton theory, using parameters characteristic of our cleaner samples, show good agreement except in the region near $\tau=0$, where the temperature-dependent part of $\delta$ has a significant effect. In that region $\sigma_{\mathrm{fl}}/\sigma_n\geqq0.5$ and neither calculation is expected to be reliable. Because of this agreement, and because the microscopic theory has been explicitly stated only for one- or two-dimensional samples, we will use Eq. (15) with the empirically determined temperature-independent $\delta$ in what follows.

Anisotropic materials will also exhibit fluctuation conductivity. The calculations[24] to date are concerned with layered materials, but in the limit of significant interlayer coupling the results are applicable to thick specimens of inherently anisotropic material. As might be expected, the temperature dependence of the fluctuation conductivity is characteristic of a three-dimensional specimen, while the magnitude depends on the current direction with respect to the preferred axis. The calculations do not consider thin films of inherently anisotropic material, nor the two- to three-dimensional crossover. Because of this limitation, and because the anisotropy of the conductivity cannot be measured in film specimens, we will not consider this case further.

## III. SPECIMEN PREPARATION AND MEASUREMENT TECHNIQUES

The specimens were prepared by vacuum evaporation onto room-temperature glass substrates. We employed three different oil-diffusion-pumped vacuum systems, each equipped with a liquid-nitrogen trap. The base pressure in all three systems was below $10^{-6}$ Torr. The basic specimen geometry was defined by suitable masks placed in contact with the substrate. Film thickness was measured by a quartz-crystal oscillator, previously calibrated by optical interferometry. After the deposition of the specimen, copper electrodes, about 1500 Å thick, were deposited through an appropriate mask to form the electrical contacts for a four-probe resistance measurement. The edges of the sample films were scraped off to eliminate shadow regions where the deposition was likely to be nonuniform.

Aluminum—aluminum-oxide specimens were made by evaporating aluminum in an oxygen atmosphere. The evaporations were performed with an electron-beam gun or a wetted tungsten filament, depending on the vacuum system used. Deposition rates of 2–20 Å/s were set and controlled by the quartz-crystal monitor. During the evaporation, the oxygen pressure was maintained at a chosen value between $5\times10^{-5}$ and $5\times10^{-4}$ Torr by steadily admitting oxygen gas into the vacuum chamber. The specimen composition, and hence the resistivity, was determined by the particular combination of evaporation rate, oxygen pressure, and source-to-substrate distance chosen.

The Al:Te specimens were made by co-depositing aluminum and tellurium at an ambient pressure of about $2\times10^{-6}$ Torr. The aluminum source was heated by an electron-beam gun. The tellurium source consisted of elemental tellurium contained in a perforated quartz tube with an external resistance heater. The two evaporation rates were controlled with independent quartz-crystal monitors.

Resistance measurements were carried out by conventional four-probe dc techniques. The maximum measuring current was 100 $\mu$A, with much smaller currents used for higher-resistivity films. Some measurements were made with the samples immersed in liquid helium with the temperature determined by the bath pressure. For the majority of the data, temperatures were determined with a calibrated germanium or carbon-glass resistance thermometer, with the specimen and the thermometer either immersed in liquid helium or thermally bonded to a heat-sunk copper block in vacuum. Magnetic fields were applied using an electromagnet or a superconducting solenoid, as needed.

To compare our measurements with models, it is necessary to define the normal-state resistivity $\rho_n$, the critical temperature $T_c$, and the critical field $H_c(T,\theta)$. Because of the presence of fluctuations which reduce the resistivity and increase the temperature width of the transition, determining these quantities requires some care. Several plausible methods exist to determine $\rho_n$: (1) extrapolate high-temperature data to the region of interest; (2) use a modest magnetic field to suppress the residual fluctuations well above $T_c$; or (3) measure $\rho(H)$ to very high fields and extrapolate to zero field. In the moderate-resistivity film specimens of interest here, these methods typically produce estimates of $\rho_n$ which differ by a few percent. We have chosen to use method (2). The critical temperature was then defined as the temperature at which the sample resistance reached half its normal-state value. The temperature width from 50–90% of the normal-state

resistance varied from 0.02 to 0.5 K, generally increasing with the sample resistance. This is a substantial fraction of $T_c$ in some cases. The critical field was similarly defined as the field needed to restore half the normal-state resistance. The critical-field data are qualitatively insensitive to this choice, as well as to the choice of $T_c$ and $\sigma_n$. The estimate of the fluctuation conductivity is more delicate.

The most direct comparison between calculated and measured fluctuation conductivities would be a plot of $\sigma_{fl}$ versus $\tau$. Testardi *et al.*[7] have discussed the problems with this approach when there are significant uncertainties in $T_c$ and $\sigma_n$. Briefly, uncertainties in $T_c$ distort the small-$\tau$ region, while uncertainties in $\sigma_n$ affect the large-$\tau$ region. They note that it is possible to avoid these problems to some extent by plotting $d(\sigma_{fl}/\sigma_n)/dT$ versus $\sigma_{fl}/\sigma_n$. This presentation eliminates the need for a determination of $T_c$ by fitting or measurement. Furthermore, normalization by $\sigma_n$ removes the film geometry from the data analysis, leaving only the small uncertainties noted above in the relative value of $\sigma/\sigma_n$. For comparison with theory, one can calculate the fluctuation conductivity from Eqs. (13)—(15), using $\xi(0)$ from the critical-field measurements. Although $T_c$ implicitly enters the equations through $\tau$, shifts of the assumed $T_c$ on the order of the transition width do not significantly alter the plot of $d(\sigma_{fl}/\sigma_n)/dT$ versus $\sigma_{fl}/\sigma_n$. Because the theoretical expressions yield a value of $\sigma_{fl}$, rather than $\sigma_{fl}/\sigma_n$, the absolute value of $\sigma_n$ enters the comparison directly, and has a large effect. This fact may allow us to learn more about the geometry of the films, at least in favorable cases.

## IV. RESULTS—Al:$Al_2O_3$ FILMS

We have examined, to varying degrees, more than fifty Al:$Al_2O_3$ specimens. The properties of the most extensively studied films are summarized in Table II. The first four columns give the identification and source of the sample, the specimen thickness, and the critical temperature. The resistance per square, $R_\square$, is derived from the measured dimensions and the resistance at 4.2 K with a perpendicular field of 15 kG applied. For comparison with other work, the apparent normal-state resistivity $\rho_n = R_\square d$ is also tabulated. The other entries will be discussed below.

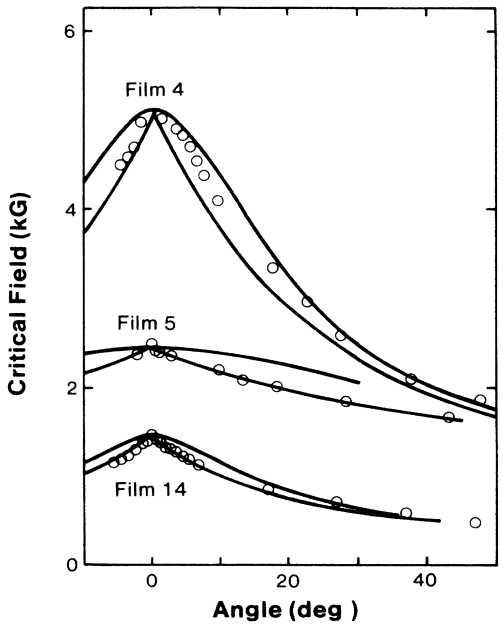


FIG. 2. Critical-field data for three films as a function of the angle between the film surface and the field. Data were obtained at $T/T_c = 0.99$, 0.96, and 0.93 for films 4, 5, and 14, respectively. The smooth curve for each film is the prediction of Eq. (5), while the cusped curve is the thin-film prediction, Eq. (1). Values of $H_{c\perp} = H_{c\perp}$ and $H_{c\parallel} = H_{c\parallel}$ were chosen to fit the data.

Figures 2—6 are intended to give an overview of our results for a wide range of film parameters. Beginning with Fig. 2, we see a relatively sharp cusp in $H_c(\theta)$ when the

TABLE II. Properties of Al:$Al_2O_3$ films

| Film | Location where work performed[a] | $d$ (Å) | $T_c$ (K) | $R_\square$ (Ω) | $\rho_n$ (Ω cm) | $\xi(0)$ (Å) | $d_{eff}$ (Å) |
|---|---|---|---|---|---|---|---|
| 1 | L | 1500 | 1.97 | 2400 | $3.6\times10^{-2}$ | 63 | 300 |
| 2 | C | 2300 | 1.80 | 1200 | $2.8\times10^{-2}$ | 58 | 680 |
| 3 | C | 2300 | 1.90 | 1130 | $2.6\times10^{-2}$ | 67 | 590 |
| 4 | R | 800 | 1.86 | 1000 | $8.0\times10^{-3}$ | 61 | 300 |
| 5 | R | 800 | 1.93 | 625 | $5.0\times10^{-3}$ | 63 | 380 |
| 6 | R | 800 | 1.98 | 500 | $4.0\times10^{-3}$ | 67 | 310 |
| 7 | L | 5000 | 2.16 | 200 | $1.0\times10^{-2}$ | 75 | 235 |
| 8 | C | 2300 | 2.20 | 52 | $1.2\times10^{-3}$ | 98 | 390 |
| 9 | C | 2300 | 2.20 | 43 | $9.9\times10^{-4}$ | 250 | 255 |
| 10 | R | 1000 | 2.06 | 30 | $3.0\times10^{-4}$ | 130 | 150 |
| 11 | L | 1680 | 2.28 | 20 | $3.3\times10^{-4}$ | 125 | 700 |
| 12 | R | 800 | 2.00 | 12 | $1.0\times10^{-4}$ | 175 | 690 |
| 13 | R | 800 | 2.06 | 12 | $1.0\times10^{-4}$ | 200 | 720 |
| 14 | R | 1000 | 2.00 | 8.0 | $8.0\times10^{-5}$ | 260 | 775 |
| 15 | C | 2300 | 2.10 | 7.0 | $1.6\times10^{-4}$ | 190 | 530 |
| 16 | L | 4500 | 1.75 | 0.2 | $1.0\times10^{-5}$ | 390 | 2000 |

[a]L, University of California, Los Angeles; C, University of Cincinnati; R, Rice University.

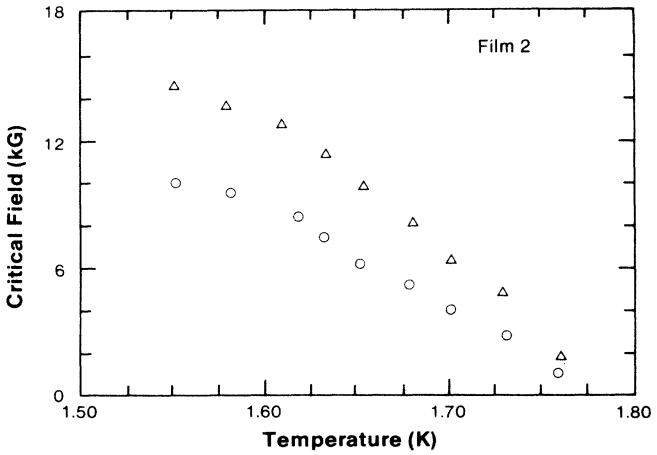


FIG. 3. Critical fields vs temperature for film 2. The triangles denote $H_{c\|}$ and the circles $H_{c\perp}$.

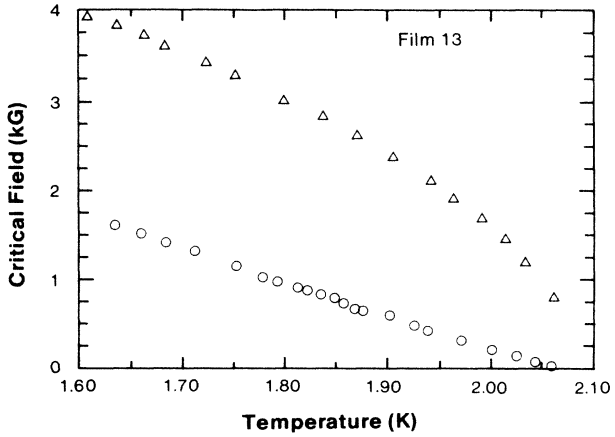


FIG. 5. Critical fields vs temperature for film 13, plotted as in Fig. 3.

applied field is parallel to the film surface. This type of angular dependence is seen in all of the films we examined, with a tendency for the cusp to be sharper in lower $R_\square$ films. Some variation from sample to sample is also evident, as, for example, in film 6, where the peak is rounded as in film 4 although the $R_\square$ is essentially identical to that of film 5,which has a clear cusp. The cusped and smooth lines are calculated for a thin film, Eq. (1), and for an anisotropic bulk specimen, Eq. (5), respectively. In both cases the measured values of $H_{c\|}$ and $H_{c\perp}$ were used. The thin-film result fits the observations better than the smooth variation of the anisotropic material. Referring to Table I, it appears that we have either a film thin compared to the coherence length, or surface superconductivity on a bulk specimen.

Turning to Figs. 3–5 we note that $H_{c\|}(T)$ is roughly parabolic, while $H_{c\perp}(T)$ is roughly linear. The slight curvature in $H_{c\perp}(T)$ varies among specimens and is rather pronounced in some; for example, Fig. 3 of Ref. 9. Similar curvature has been seen in deliberately layered films,[25] but the origin of the effect is not known. A plot of $H_{c\perp}/H_{c\|}$, Fig. 6, is approximately linear near $T_c$, reaching a plateau at low temperature for some films. All of these facts are consistent with a sample consisting of one or more layers which are thin compared with the coherence length near $T_c$ (see Table I). At lower temperatures some of the specimens apparently enter the three-dimensional regime as $\xi(T)$ decreases, and exhibit surface superconductivity.

Adopting the thin-film model, we can make the argument more quantitative. The slope $dH_{c\perp}/dT$ gives $\xi(0)$ through Eq. (3), while the effective film thickness $d_{\text{eff}}$ can be found from Eq. (4). The results of these calculations are listed in Table II. As previously noted for this system,[9] the effective thicknesses needed to account for the

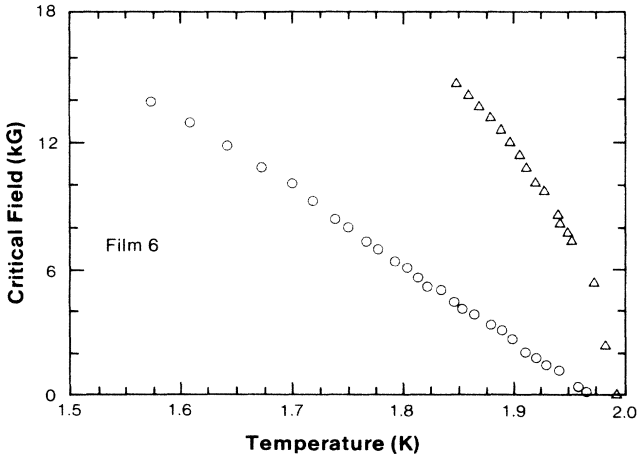


FIG. 4. Critical fields vs temperature for film 6, plotted as in Fig. 3.

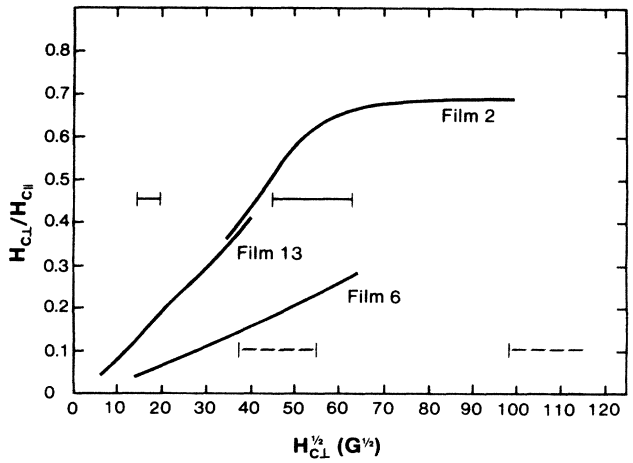


FIG. 6. Plot of $H_{c\perp}/H_{c\|}$ vs $H_{c\perp}^{1/2}$ for three films. The data were obtained by interpolation of plots of $H_{c\perp}(T)$ and $H_{c\|}(T)$. The solid bar at small $H_{c\perp}^{1/2}$ marks the two- to three-dimensional transition region predicted for film 2 by use of the full film thickness $d$, while the solid bar at large $H_{c\perp}^{1/2}$ marks the transition calculated using $d_{\text{eff}}$. The two dashed bars represent the corresponding estimates for film 6. For film 13, both calculated transition regions are above the range of the data and are not marked.

critical-field data are substantially less than the film thicknesses in many cases.

We can check the consistency of our estimate of $d_{\rm eff}$ by using the numerical results contained in Fig. 1 to estimate the critical-field value at which the two- to three-dimensional transition should occur. If we use $d$, the macroscopic thickness of the film, we predict that essentially all the films should exhibit the two- to three-dimensional transition in our temperature and field range. This is not, in fact, true, as shown in Fig. 6. Only one film of the three shown displays the low-temperature plateau expected from surface superconductivity, and that occurs at a much higher $H_{c\perp}$ than the estimate. When we repeat the calculation of the transition fields using $d_{\rm eff}$, we predict that the dimensional changeover should be observable only in films 2, 3, and 12. A transition to a plateau is, in fact, observed at the calculated fields for all three of these films, and is shown for film 2 in Fig. 6. We note that $H_{c\perp}/H_{c\parallel}$ becomes approximately constant at a value near 0.7, substantially above the expected value of 0.59 for the ratio $H_{c2}/H_{c3}$. The paramagnetic limiting parameter $\alpha$, estimated from Eqs. (10)—(12), is $\approx 2.8$ for this film, so the observed increase in the plateau value is reasonable.[13] The paramagnetic limiting effect is also observed in film 3, while limiting is neither predicted nor observed in film 12. It appears that the data are adequately accounted for by the assumption of a layer of isotropic superconductor which is substantially thinner than the overall film.

The fluctuation-conductivity measurements above $T_c$, displayed in Figs. 7 and 8, can be used to corroborate this model. The plotted points were obtained by numerically differentiating point-by-point conductivity data over the temperature range from 4.2 K to $T_c$. As noted above, the geometric factors which connect resistance to conductivity cancel in the ratio $\sigma_{\rm fl}/\sigma_n=(\sigma-\sigma_n)/\sigma_n$, so the only remaining difficulty is in the estimate of the normal-state resistance. Application of a 15-kG field may not totally suppress the fluctuations, especially in the higher-resistivity films, so we expect to overestimate $\sigma_n$. This would produce a concave-upward curvature at small $\sigma_{\rm fl}/\sigma_n$. In the plots, $\sigma_n$ has been decreased by up to 2% as noted in the captions, to obtain better agreement with the calculated lines at low $\sigma_{\rm fl}/\sigma_n$. This adjustment has essentially no effect for most of the range of the data plotted, and therefore does not significantly affect our comparison with the calculation. It is, of course, also possible that the curvature observed in many of our specimens occurs because $\sigma_{\rm fl}$ decreases at large $\tau$ more rapidly than calculated, but we have no evidence to support this conjecture.

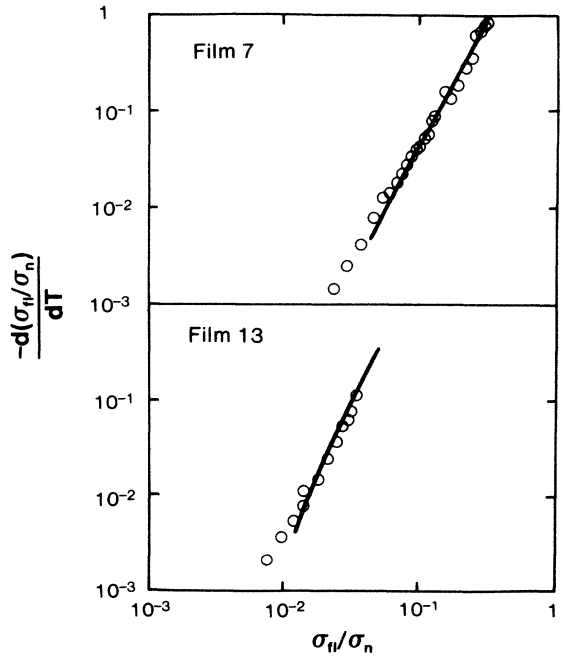


FIG. 7. Fluctuation-conductivity data for two low-resistivity films. The points were obtained by numerically differentiating the conductivity data. As discussed in the text, the measured $\sigma_n$ was decreased by 2% for film 7 and by 0.2% for film 13. The solid lines were calculated from Eq. (15).

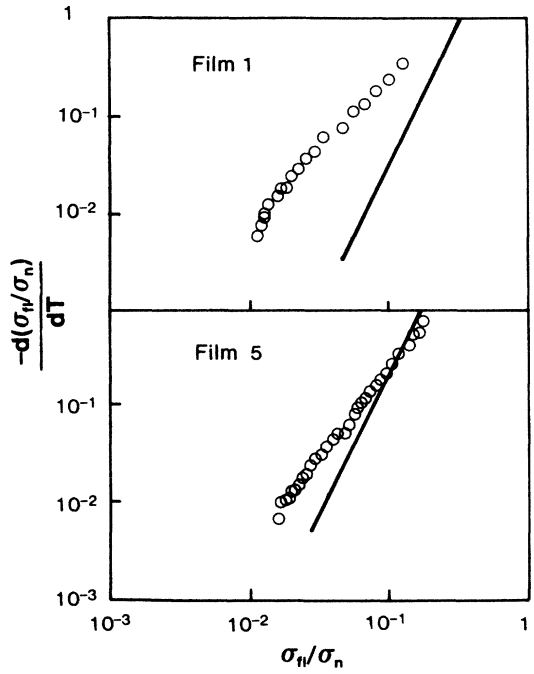


FIG. 8. Fluctuation-conductivity data for two higher-resistivity films. The measured $\sigma_n$ was unchanged for film 1, and decreased by 2% for film 5. The solid lines represent only the Aslamazov-Larkin contribution to $\sigma_{\rm fl}$.

The fluctuation conductivity is calculated from Eqs. (13)—(15), using $\xi(0)$, $d$, and $T_c$ from Table II. The pair-breaking parameter has been previously determined[1] to be $\delta\approx(3+6R_\square)\times10^{-4}$ for very thin aluminum films with $R_\square<200\ \Omega$. We consider two limiting cases to estimate $\sigma_n$ from the tabulated $R_\square$ and thickness. If the film consists of one layer of thickness $d_{\rm eff}$, then $\sigma_n'=1/R_\square d_{\rm eff}$. If the film consists of several layers which together comprise the film thickness, then $\sigma_n=1/R_\square d$. The difference between these estimates can be substantial.

The calculated fluctuation conductivity is shown as solid lines in Figs. 7 and 8. The two films in Fig. 7 have relatively low resistivity, so the full expression of Eq. (15)

can be used with the empirical values of $\delta$. The lines shown are for $\sigma_n'$, the single-layer conductivity. Since $d \approx d_{\text{eff}}$ for film 13, the distinction between $\sigma_n$ and $\sigma_n'$ is unimportant, but for film 7 the two estimates differ by a factor of 21. If $\sigma_n$ had been used for film 7, the calculation would greatly overestimate the width of the transition and the solid line would be displaced to the right by nearly a full decade. The same observations hold for the other films with $R_\square < 200\ \Omega$. It appears, therefore, that the transition width in our cleaner films is adequately described by Eq. (15) if we assume that they consist of a single electrically active layer.

Calculated results for two higher-resistivity films are shown in Fig. 8. The empirical expression for $\delta$ is certainly not valid at large $R_\square$, so the solid lines are calculated from the Aslamazov-Larkin terms only, using Eq. (13) and $\sigma_n'$. Inclusion of Maki-Thompson terms or the use of $\sigma_n$ rather than $\sigma_n'$ would shift the lines to the right. Our calculation, therefore, seriously overestimates the width of the resistive transition in the higher-resistivity specimens. The reason for this discrepancy, which generally increases with increasing $R_\square$, is not understood. One can speculate that the internal geometry of the film is changing from a simple layer structure to a more complex but still planar arrangement of conduction paths. Unfortunately, independent confirmation of this picture is likely to be difficult.

## V. RESULTS—Al:Te FILMS

We have measured the angular dependence of the critical fields on about twenty-five Al:Te films of varied resistivity and thickness. We have also obtained some data on the temperature dependence of $H_c$ and $\sigma$. The behavior of these films is much more complex and less reproducible than that of the Al:$Al_2O_3$ films. Work on this system is continuing, but we present some preliminary results here for purposes of comparison.

Thin low-resistivity Al:Te films [less than about 400 Å with $\rho_n = (1-10)\times 10^{-4}\ \Omega\,\text{cm}$] display a cusp in $H_c(\theta)$. The temperature dependence $H_{c\parallel}(T)$ is roughly parabolic, while $H_{c\perp}(T)$ is approximately linear, with a slight concave-upward curvature in some samples. The fluctuation conductivity is in reasonable agreement with Eq. (15), using the film thickness $d$, and $\xi(0)$ from the perpendicular critical-field measurements. Lacking any better information, the pair-breaking parameter $\delta$ was estimated from $R_\square$, using the same parameters as for the oxide films. It seems reasonable to conclude that these low-resistivity films can be adequately described as dirty type-II superconductors, as one might expect.

Thicker films, 2000—4000 Å, of about the same resistivity, exhibit more variability. The first example is presented in Fig. 9, which shows the angular dependence of $H_c$ at two temperatures. There is a smooth peak when the field is nearly perpendicular to the substrate ($\theta = 90°$) and no sign of a cusp near the parallel orientation. The ratio $H_{c\perp}/H_{c\parallel} \approx 2.6$ is approximately independent of temperature. Referring to Table I, this angular dependence is consistent with geometric limiting of the screening currents around two axes, although the ratio of critical

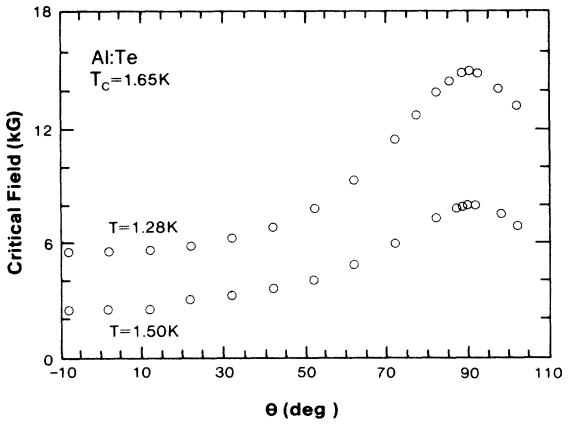


FIG. 9. Critical-field data for an Al:Te film ($\rho_n = 1.8\times 10^{-3}$ $\Omega$ cm, $d = 2000$ Å) as a function of the angle between the film surface and the field.

fields is bigger than calculated for isolated cylinders. We also find that the critical fields $H_{c\perp}(T)$ and $H_{c\parallel}(T)$ are concave downward, as expected for geometric limiting. Together, these data suggest that this film is composed of weakly coupled columns or cylinders with their axes oriented normal to the substrate. Similar critical-field anisotropy effects seen in other thin-film systems have also been attributed to columnar structures,[26] and a large-scale columnar morphology is often observed by microscopy in films deposited in such a way that atomic mobility is limited.[27]

Our second example, shown in Fig. 10, displays a cusp at the parallel orientation and a smooth peak at the perpendicular orientation. There are at least two possible explanations for this angular dependence. The simplest is that the film is composed of two parts, one with a columnar microstructure similar to that of the film in Fig. 9,

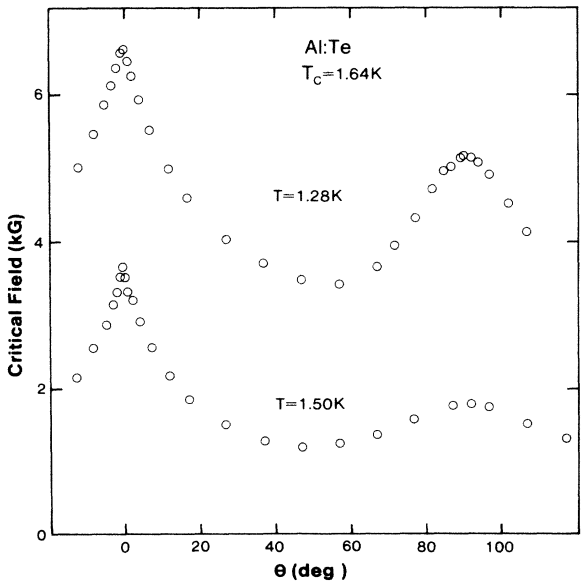


FIG. 10. Critical-field data as in Fig. 9 for an Al:Te film ($\rho_n = 4.0\times 10^{-4}\ \Omega$ cm, $d = 4500$ Å).

and another which is a thin layer. If current can pass through both parts of the film, we would obtain the measured angular dependence. Alternatively, the basic structure might be columnar with some sort of surface superconductivity across the ends of the weakly coupled columns persisting to high field. On the basis of the available data it is not possible to decide between these alternatives, or to rule out other explanations.

## VI. SUMMARY AND CONCLUSIONS

We have presented critical-field and fluctuation-conductivity data on Al:$Al_2O_3$ films made in three different evaporators over a long span of time. The film properties are remarkably consistent from specimen to specimen, but are not accounted for by the assumption of complete homogeneity on the scale of the coherence length. Rather, many of the superconducting properties can be understood by assuming that the specimens contain a conducting layer much thinner than the film. It is not clear from our measurements if there are several such layers, or only one active layer surrounded by electrically inactive material. In the higher-resistivity samples the internal geometry may be more complicated, as shown by the disagreement between the measured and calculated "fluctuation conductivity."

Similar but less extensive measurements on Al:Te films indicate that a large-scale microstructure is also present in this system. The observed critical fields could be due to a columnar morphology, as previously suggested for another system,[26] but no attempt has been made to model the structure in detail. It also appears that the morphology of the Al:Te films is more sensitive to preparation details than is the case for the oxide films.

Finally, we note that measurements of $H_c(\theta,T)$ can be made to yield a good deal of information about the structure of superconducting composite materials. When feasible, it should therefore prove useful to employ critical-field measurements as a tool for characterizing composite materials intended for use in other investigations.

## ACKNOWLEDGMENTS

One of us (R.S.N.) would like to acknowledge the support of the National Science Foundation (Grant No. DMR-84-41254) and the University of Cincinnati Research Council.

## APPENDIX: CRITICAL FIELDS FOR A CYLINDER

We consider a superconducting, right circular cylinder of radius $R$ small compared to the coherence length $\xi(T)$. An external field is applied at an angle $\theta$, measured from a plane perpendicular to the cylinder axis. We use cylindrical coordinates $(r,\phi,z)$ and we wish to solve the linearized Ginzburg-Landau equation[12]

$$\left[\frac{\nabla}{i}-\frac{2\pi\mathbf{A}}{\phi_0}\right]^2\Psi=\frac{1}{\xi^2(T)}\Psi \tag{A1}$$

subject to the boundary condition

$$\left[\frac{\hbar}{i}\nabla-\frac{e^*}{c}\mathbf{A}\right]\Psi\Big|_n=0\,, \tag{A2}$$

with $\mathbf{H}=\nabla\times\mathbf{A}$ and $\nabla\cdot\mathbf{A}=0$ (London gauge). Since $\xi(T)\gg R$ we may assume $\Psi$ only depends on $z$. In that case, $A_r=0$, $A_\phi=\frac{1}{2}Hr\sin\theta$, and $A_z=Hr\cos\theta\sin\phi$ is a suitable choice for the vector potential. Note that this potential satisfies both the boundary condition and the gauge. Equation (A1) becomes

$$-\nabla^2\Psi+\frac{4\pi i}{\phi_0}\mathbf{A}\cdot\nabla\Psi+\frac{4\pi^2A^2}{\phi_0^2}\Psi=\frac{1}{\xi^2(T)}\Psi\,. \tag{A3}$$

Following Tinkham,[12] we can replace $r^2$, $r^2\sin\phi$, and $r\sin\phi$ by their averages, yielding

$$\frac{\partial^2\Psi}{\partial z^2}=\left[\left[\frac{\pi HR}{\phi_0}\right]^2\left(\tfrac{1}{2}\sin^2\theta+\cos^2\theta\right)-\frac{1}{\xi^2(T)}\right]\Psi$$

$$=\Gamma(\theta,H)\Psi\,. \tag{A4}$$

(The same answer follows from a careful variational calculation in this case, exactly as Tinkham notes for the plane.) Equation (A4) has solutions

$$\Psi=\pm a\exp[\pm\sqrt{\Gamma(\theta,H)}z]\,. \tag{A5}$$

Acceptable solutions must be bounded, requiring $\Gamma<0$. Since $\Gamma>0$ for large $H$, the first solution occurs when $\Gamma=0$ or

$$H_c(\theta)=\frac{\phi_0}{\pi R\xi(T)}\left(\tfrac{1}{2}\sin^2\theta+\cos^2\theta\right)^{-1/2}\,. \tag{A6}$$

Two special cases are

$$H_c(\theta=0)=H_{ct}=\frac{\phi_0}{\pi R\xi(T)} \tag{A7}$$

and

$$H_c(\theta=\pi/2)=H_{cz}=\sqrt{2}\frac{\phi_0}{\pi R\xi(T)}\,. \tag{A8}$$

The ratio of critical fields, $\sqrt{2}$, agrees with previous calculations.[28]

---

*Current address: Central Engineering Department, Conoco Inc., Ponca City, OK 74601.

†Current address: Magnetic Peripherals, Inc., Minneapolis, MN 55435.

[1]W. J. Skocpol and M. Tinkham, Rep. Prog. Phys. 38, 1049 (1975).

[2]The following are a few of the many studies done to date: M. Beasley, T. Orlando, and H. Mooij, Phys. Rev. Lett. 42, 1165 (1979); K. Epstein, A. M. Goldman, and A. M. Kadin, *ibid.* 47, 534 (1981); R. C. Dynes, J. P. Garno, and J. M. Rowell, *ibid.* 40, 479 (1978); D. U. Gubser and S. A. Wolf, Solid State Commun. 32, 449 (1979); S. A. Wolf, D. U. Gubser, W.

W. Fuller, J. C. Garland, and R. S. Newrock, Phys. Rev. Lett. **47**, 1071 (1981); A. F. Hebard and A. T. Fiory, *ibid.* **44**, 291 (1981); R. F. Voss, C. M. Knoedler, and P. M. Horn, *ibid.* **45**, 1523 (1980).

[3]Among others, the following used granular materials: T. Chui, P. Lindenfeld, W. L. McLean, and K. Mui, Phys. Rev. Lett. **47**, 1617 (1981); A. F. Hebard and J. M. Vandenberg, *ibid.* **44**, 50 (1980); J. M. Vandenberg, S. Nakahara, and A. F. Hebard, J. Vac. Sci. Technol. **18**, 268 (1981).

[4]Typical studies using granular materials include T. Chui, G. Deutscher, and W. L. McLean, Phys. Rev. B **23**, 6172 (1981); R. C. Dynes and J. P. Garno, Phys. Rev. Lett. **46**, 137 (1981).

[5]G. Deutscher, H. Fenichel, M. Gershenson, E. Grunbaum, and Z. Ovadyahu, J. Low Temp. Phys. **10**, 231 (1973).

[6]B. Abeles, P. Sheng, M. D. Coutts, and Y. Arie, Adv. Phys. **24**, 407 (1975).

[7]L. R. Testardi, W. A. Reed, P. C. Hohenberg, W. H. Haemmerle, and G. F. Brennert, Phys. Rev. **181**, 800 (1969).

[8]A small sample of the extensive literature would include P. A. Bancel and K. E. Gray, Phys. Rev. Lett. **46**, 148 (1981); K. E. Gray and I. Schuller, J. Low Temp. Phys. **28**, 75 (1977); G. Deutscher, Physica **109&110B+C**, 1629 (1982); S. Cremer and E. Simanek, Phys. Rev. B **14**, 1927 (1976); Solid State Commun. **22**, 405 (1977); Yu. M. Galperin, V. I. Kozub, Z. G. Medoeva, and A. S. Skal, Fiz. Tverd. Tela. (Leningrad) **22**, 248 (1980) [Sov. Phys.—Solid State **22**, 146 (1980)]; M. Gershenson and W. L. McLean, J. Low Temp. Phys. **47**, 123 (1982); R. B. Laibowitz, E. I. Allessandrini, and G. Deutscher, Phys. Rev. B **25**, 2965 (1982); K. A. Muller, M. Pomerantz, C. M. Knoedler, and D. Abraham, Phys. Rev. Lett. **45**, 832 (1980); W. L. McLean, Phys. Rev. B **22**, 456 (1980).

[9]G. Deutscher and S. A. Dodds, Phys. Rev. B **16**, 3936 (1977).

[10]R. W. Cohen and B. Abeles, Phys. Rev. **168**, 444 (1968); T. Chui, P. Lindenfeld, W. L. McLean, and K. Mui, Phys. Rev. B **24**, 6728 (1981).

[11]N. R. Werthamer, in *Superconductivity,* edited by R. D. Parks (Dekker, New York, 1969).

[12]M. Tinkham, *Introduction to Superconductivity* (McGraw-Hill, New York, 1975).

[13]D. St. James, G. Sarma, and E. J. Thomas, *Type II Superconductivity* (Pergamon, Oxford, 1969).

[14]H. J. Fink, Phys. Rev. **177**, 732 (1969).

[15]W. E. Lawrence and S. Doniach, in *Proceedings of the 12th International Conference on Low Temperature Physics (Kyoto, Japan, 1970),* edited by E. Kanda (Keigaku, Tokyo, 1971) p. 361; R. A. Klemm, A. Luther, and M. R. Beasley, Phys. Rev. B **12**, 877 (1975).

[16]D. R. Tilley, Proc. Phys. Soc. London **85**, 1177 (1965).

[17]P. M. Tedrow and R. Meservey, Phys. Rev. Lett. **43**, 384 (1979).

[18]L. G. Aslamazov and A. I. Larkin, Fiz. Tverd. Tela. (Leningrad) **10**, 1104 (1968) [Sov. Phys.—Solid State **10**, 875 (1968)]; Phys. Lett. **26A**, 238 (1968).

[19]R. S. Thompson, Phys. Rev. B **1**, 327 (1970).

[20]B. R. Patton, Phys. Rev. Lett. **27**, 1273 (1971); B. R. Patton, in *Proceedings of the Thirteenth International Conference on Low Temperature Physics, Boulder, Colorado, 1972,* edited by W. J. O'Sullivan, K. D. Timmerhaus, and E. F. Hammel (Plenum, New York, 1974), Vol. 3, p. 642.

[21]J. Keller and V. Korenman, Phys. Rev. B **5**, 4367 (1972).

[22]J. M. Gordon, C. J. Lobb, and M. Tinkham, Phys. Rev. B **29**, 5232 (1984).

[23]R. A. Craven, G. A. Thomas, and R. D. Parks, Phys. Rev. B **7**, 157 (1973).

[24]R. A. Klemm, J. Low Temp. Phys. **16**, 381 (1974); L. G. Aslamasov and A. A. Varlamov, *ibid.* **38**, 223 (1980).

[25]T. W. Haywood and D. G. Ast, Phys. Rev. B **18**, 2225 (1978); S. T. Ruggiero, T. W. Barbee, Jr., and M. R. Beasley, *ibid.* **26**, 4894 (1982).

[26]H. F. Braun, E. N. Haeussler, and E. J. Saur, J. Less-Common Met. **62**, 95 (1978); A. S. Sidorenko, E. V. Minenko, N. Ya. Fogel, R. I. Shekter, and I. O. Kulik, Phys. Status Solidi A **52**, K89 (1979).

[27]A. G. Dirks and H. J. Leamy, Thin Solid Films **47**, 219 (1977).

[28]J. Bardeen, Rev. Mod. Phys. **34**, 667 (1962).